

# Atmospheric NO<sub>2</sub>: In Situ Laser-Induced Fluorescence Detection at Parts per Trillion Mixing Ratios

Joel A. Thornton,<sup>†</sup> Paul J. Wooldridge,<sup>†</sup> and Ronald C. Cohen<sup>\*,†,‡,§</sup>

Department of Chemistry, University of California, Berkeley, Berkeley, California 94720, Department of Geology and Geophysics, University of California, Berkeley, and Energy and Environment Technologies Division, Lawrence Berkeley National Laboratory

**We describe a time-gated laser-induced fluorescence instrument designed for accurate ( $\pm 5\%$ ,  $1\sigma$ ), continuous, autonomous, in situ observations of NO<sub>2</sub> with the sensitivity (15 ppt/10 s at S/N = 2) and portability necessary to study NO<sub>2</sub> anywhere in the troposphere. The technique is advantageous because it is spectroscopically specific and direct in that it does not require conversion of NO<sub>2</sub> into another species (e.g., NO) prior to detection, eliminating a class of potential interferences. Performance of the instrument is illustrated with 15 weeks (July–Oct 1998) of observations at the University of California, Blodgett Forest field station located in the foothills of the Sierra Nevada and 4 weeks (June 15 – July 15, 1999) in Nashville, TN during the Southern Oxidants Study. Ambient concentrations of NO<sub>2</sub> at Blodgett Forest varied from below 50 ppt to 4000 ppt and NO<sub>x</sub> ranged from 5 to 50% of the total reactive nitrogen; while in Nashville, TN, concentrations ranged from 1 to 75 ppb.**

The oxides of nitrogen, NO and NO<sub>2</sub> (NO<sub>x</sub>  $\equiv$  NO + NO<sub>2</sub>), play a central role in atmospheric chemistry, regulating production rates of ozone and OH in the troposphere<sup>1</sup> and destruction rates of ozone in the stratosphere.<sup>2</sup> Processes that exchange NO<sub>x</sub> and its oxidation products between the surface (soils, rivers, etc.) and the atmosphere are important to global and regional ecology<sup>3</sup> and may be a significant factor in the regulation of terrestrial carbon uptake by nitrogen-limited forests.<sup>4</sup> Gas-phase NO<sub>x</sub> has also been shown to initiate seed germination in fire-sensitive species,<sup>5</sup> thus

raising the interesting possibility that NO<sub>x</sub> emissions may be substantially altering some ecosystems through species-specific biochemical mechanisms as well as by the more commonly recognized effects of nitrate on the nutrient balance and acid rain on the pH balance. Our need to understand these processes is increasing as a result of the enormous growth in anthropogenic NO<sub>x</sub> emissions. Anthropogenic NO<sub>x</sub> emissions are now estimated to be 3–4 times natural emissions, and they are expected to double again by 2020.<sup>6</sup> Changes to NO<sub>x</sub> have affected, and will continue to affect, atmospheric chemistry and composition on local, regional, and global scales.

In urban areas, NO<sub>x</sub> mixing ratios of 10–100 parts per billion are typical,<sup>7</sup> while in the remote atmosphere, concentrations of a few parts per trillion have been measured.<sup>8,9</sup> Techniques used to measure NO at atmospherically relevant mixing ratios (1 ppt – 10 ppb), including O<sub>3</sub>-chemiluminescence<sup>10</sup> and two-photon laser-induced fluorescence are accurate (5%), sensitive, and have small uncertainties in their zero.<sup>11</sup> In contrast, existing techniques for measuring NO<sub>2</sub> are generally less accurate and reliable, especially at concentrations below 1000 ppt and in environments where higher oxides of nitrogen are more abundant by factors of 10–100.<sup>12</sup> In this paper, we describe the design, development, and initial field trials of a laser-induced fluorescence (LIF) instrument that provides a new, reliable, and accurate method for detection of NO<sub>2</sub> throughout the atmosphere. The instrument offers the advantages of high sensitivity, high accuracy, and immunity from interferences associated with photochemical conversion of NO<sub>2</sub> to another species prior to detection. It is designed to be capable

\* Corresponding author: (tel.) 510-642-2735; (fax) 510-642-6911; C (e-mail) Cohen@cchem.berkeley.edu.

<sup>†</sup> Department of Chemistry, University of California, Berkeley.

<sup>‡</sup> Department of Geology and Geophysics, University of California, Berkeley.

<sup>§</sup> Lawrence Berkeley National Laboratory.

- (1) Logan, J. A.; Prather, M. J.; Wofsy, S. C.; McElroy, M. B. *J. Geophys. Res.* **1981**, *86*, 7210–7254.
- (2) Wennberg, P. O.; Cohen, R. C.; Stimpfle, R. M.; Koplow, J. P.; Anderson, J. G.; Salawitch, R. J.; Fahey, D. W.; Woodbridge, E. L.; Keim, E. R.; Gao, R. S.; Webster, C. R.; May, R. D.; Toohey, D. W.; Avallone, L. M.; Proffitt, M. H.; Loewenstein, M.; Podolske, J. R.; Chan, K. R.; Wofsy, S. C. *Science (Washington, D.C.)* **1994**, *266*, 398–404.
- (3) Pelley, J. *Environ. Sci. Technol.* **1998**, *32*, 462–466.
- (4) Holland, E. A.; Braswell, B. H.; Lamarque, J. F.; Townsend, A.; Sulzman, J.; Muller, J. F.; Dentener, F.; Brasseur, G.; Levy, H., II.; Penner, J. E.; Roelofs, G. J. *J. Geophys. Res.* **1997**, *102*, 15849–15866.
- (5) Keeley, J. E.; Fotheringham, C. J. *Science (Washington, D.C.)* **1997**, *276*, 1248–1250.

- (6) Yienger, J. J.; Klonecki, A. A.; Levy, H.; Moxim, W. J.; Carmichael, G. R. *J. Geophys. Res., Atmos.* **1999**, *104*, 3655–3667, and references therein.

- (7) NAS. *Rethinking the ozone problem in urban and regional air pollution*; National Academy Press: Washington, D. C., 1991.

- (8) Carroll, M. A.; Ridley, B. A.; Montzka, D. D.; Hubler, G.; Walega, J. G.; Norton, R. B.; Huebert, B. J.; Grahek, F. E. *J. Geophys. Res.* **1992**, *97*, 10361–10374.

- (9) Crawford, J. H.; Davis, D. D.; Chen, G.; Bradshaw, J.; Sandholm, S.; Kondo, Y.; Merrill, J.; Liu, S.; Browell, E.; Gregory, G.; Anderson, B.; Sachse, G.; Barrick, J.; Blake, D.; Talbot, R.; Poeschel, R. *J. Geophys. Res.* **1997**, *102*, 28447–28468.

- (10) e.g. Ridley, B. A.; Walega, J. G.; Dye, J. E.; Grahek, F. E. *J. Geophys. Res.* **1994**, *99*, 25519–25534.

- (11) Sandholm, S.; Smyth, S.; Bai, R.; Bradshaw, J. *J. Geophys. Res.* **1997**, *102*, 28651–28661.

- (12) Crawford, J.; Davis, D.; Chen, G.; Bradshaw, J.; Sandholm, S.; Gregory, G.; Sachse, G.; Anderson, B.; Collins, J.; Blake, D.; Singh, H.; Heikes, B.; Talbot, R.; Rodriguez, J. *J. Geophys. Res.* **1996**, *101*, 2053–2072.

of making observations from the surface to 40 km, and it contains a series of internal standards to aid in maintaining a precise calibration over months to years. As a result of these features and rapid progress in laser technology, over the next few years we expect this instrument will evolve into a small, lightweight, fully autonomous, inexpensive sensor capable of routine measurements of NO<sub>2</sub> from aircraft, balloons, and ground stations.

Before describing our new instrument in detail, we briefly review some other approaches to NO<sub>2</sub> detection. This discussion emphasizes techniques that have been subject to an atmospheric field trial. There are numerous other techniques that have shown promise in the laboratory (e.g., surface acoustic wave detectors<sup>13</sup>) under highly controlled conditions. Without a field trial, it is difficult to evaluate the specificity of these methods and their potential to suffer from interferences at concentrations of interest in the atmosphere. The most common technique used to measure atmospheric NO<sub>2</sub> is Photo-Fragmentation Chemi-Luminescence, hereafter PF-CL, in which photolytic conversion of NO<sub>2</sub> to NO is followed by chemiluminescence detection of NO.<sup>14–21</sup> Photolysis of NO<sub>2</sub> is accomplished using UV light from a filtered xenon arc lamp ( $\lambda \sim 375$  nm) in a flowing sample. O<sub>3</sub> is added to the sample flow downstream of the photolysis cell where it reacts with NO to produce electronically excited NO<sub>2</sub>. The excited NO<sub>2</sub>\* emits a broad continuum of radiation peaking at 1.3  $\mu\text{m}$ .<sup>22</sup> The visible portion of this emission 500–900 nm is detected using a red-sensitive photomultiplier tube (PMT). Such instruments are commercially available (e.g., Eco Physics, Inc., Ann Arbor, MI) with detection limits of 155 ppt/10 s,<sup>23</sup> and custom-built versions have reached still lower detection limits. For example, Del Negro et al. have demonstrated a sensitivity near 25 ppt/10 s with an accuracy ranging from  $\pm 10$ –30%.<sup>21,24</sup> For the ease of comparisons, count rates and sensitivities will be reported as those achieved in 10-s integration periods at a signal-to-noise ratio of 2:1. We assume

that the sensitivity of these other instruments scales as the square root of the integration time and adjust values as reported in the literature accordingly.

Bradshaw et al. use two-photon laser-induced fluorescence in place of the O<sub>3</sub>-chemiluminescence reaction to measure NO derived from the photolysis of NO<sub>2</sub>. In a recent study, they report a detection limit for NO<sub>2</sub> of 8 ppt/10 s for the Photo-Fragmentation Two-Photon Laser-Induced Fluorescence (PF-TP-LIF) instrument which uses the third harmonic of an Nd<sup>3+</sup>:YAG laser for the photolysis of NO<sub>2</sub> and two-photon excitation to the C state of NO followed by fluorescence as a means of NO detection.<sup>25</sup> In a number of studies, the accuracy of this instrument has been questioned because of possible interferences.<sup>12,26</sup> Bradshaw et al. have attributed the interferences to surface decomposition of other NO<sub>2</sub> containing species and have tried to minimize the effect by increasing the sample flow rate. However, several of these species, such as peroxyacetylnitrate (PAN), considered to be the largest interference, are commonly detected using gas chromatography, a method that depends directly on the molecule surviving numerous collisions with surfaces, suggesting that surface decomposition is not likely to be the primary source of the observed interference.

Both the PF-CL and PF-TP-LIF detection methods are sensitive enough for observation of NO<sub>2</sub> anywhere on the globe. Their shortcomings arise from: (a) the indirect nature of the photolysis step and consequent additional uncertainty about how the instrument will respond to other NO<sub>2</sub> containing compounds, (b) the requirement for a simultaneous NO measurement and the associated need to determine NO<sub>2</sub> as the difference between NO<sub>x</sub> and NO, (c) the large size, weight, and electrical power consumption of these instruments, and (d) the difficulty of translating the performance of scientific instruments to commercially available ones that can be operated routinely at the high data quality characteristic of research-grade instrumentation.

Another commonly used technique for NO<sub>2</sub> detection is the luminol-chemiluminescence method, first developed by Wendel et al. in 1983.<sup>27</sup> Instruments based on this method are commercially available, and they have been used by several groups to measure atmospheric NO<sub>2</sub>,<sup>16</sup> NO<sub>x</sub> fluxes by eddy correlation,<sup>28</sup> and NO<sub>2</sub> derived from thermal decomposition of PAN and other organic nitrates.<sup>29,30</sup> The technique employs reaction between NO<sub>2</sub> and a solution of luminol resulting in fluorescence peaking near 425 nm. The technique is direct and sensitive (part-per-trillion detection limits), but it is nonspecific. O<sub>3</sub>, PAN, and other peroxy nitrates are detected with high and sometimes variable efficiency.<sup>16</sup> Gaffney et al. have recently reported a gas chromatographic separation of NO<sub>2</sub> and C<sub>2</sub>–C<sub>4</sub> peroxy nitrates, followed by detection using luminol with part-per-trillion sensitivity.<sup>31</sup>

- (13) Penza, M.; Vasanelli, L. *Sens. Actuators, B* **1997**, *B41*, 31–36.
- (14) Fahey, D. W.; Hubler, G.; Parrish, D. D.; Williams, E. J.; Norton, R. B.; Ridley, B. A.; Singh, H. B.; Liu, S. C.; Fehsenfeld, F. C. *J. Geophys. Res.* **1986**, *91*, 9781–9793.
- (15) Ridley, B. A.; Carroll, M. A.; Gregory, G. L.; Sachse, G. W. *J. Geophys. Res.* **1988**, *93*, 15813–15830.
- (16) Fehsenfeld, F. C.; Drummond, J. W.; Roychowdhury, U. K.; Galvin, P. J.; Williams, E. J.; Buhr, M. P.; Parrish, D. D.; Hubler, G.; Langford, A. O.; Calvert, J. G.; Ridley, B. A.; Grahek, F.; Heikes, B. G.; Kok, G. L.; Shetter, J. D.; Walega, J. G.; Elsworth, C. M.; Norton, R. B.; Fahey, D. W.; Murphy, P. C.; Hoovermale, C.; Mohnen, V. A.; Demerjian, K. L.; Mackay, G. I.; Schiff, H. I. *J. Geophys. Res.* **1990**, *95*, 3579–3597.
- (17) Munger, J. W.; Wofsy, S. C.; Bakwin, P. S.; Song-Miao, F.; Goulden, M. L.; Daube, B. C.; Goldstein, A. H.; Moore, K. E.; Fitzjarrald, D. R. *J. Geophys. Res.* **1996**, *101*, 12639–12657.
- (18) Harder, J. W.; Williams, E. J.; Baumann, K.; Fehsenfeld, F. C. *J. Geophys. Res.* **1997**, *102*, 6227–6243.
- (19) Williams, E. J.; Roberts, J. M.; Baumann, K.; Bertman, S. B.; Buhr, S.; Norton, R. B.; Fehsenfeld, F. C. *J. Geophys. Res.* **1997**, *102*, 6297–6314.
- (20) Dias-Lalcaca, P.; Brunner, D.; Imfeld, W.; Moser, W.; Staehelin, J. *Environ. Sci. Technol.* **1998**, *32*, 3228–3236.
- (21) Gao, R. S.; Keim, E. R.; Woodbridge, E. L.; Ciciora, S. J.; Proffitt, M. H.; Thompson, T. L.; McLaughlin, R. J.; Fahey, D. W. *J. Geophys. Res.* **1994**, *99*, 20673–20681.
- (22) Clough, P. N.; Thrush, B. A. *Trans. Faraday Soc.* **1967**, *63*, 915–925.
- (23) Dias-Lalcaca, P.; Brunner, D.; Imfeld, W.; Moser, W.; Staehelin, J. *Environ. Sci. Technol.* **1998**, *32*, 3228–3236.
- (24) Del Negro, L. A.; Fahey, D. W.; Gao, R. S.; Donnelly, S. G.; Keim, E. R.; Neuman, J. A.; Cohen, R. C.; Perkins, K. K.; Koch, L. C.; Salawitch, R. J.; Lloyd, S. A.; Proffitt, M. H.; Margitan, J.; Stimpfle, R. M.; Bonne, G. P.; Voss, P. B.; Wennberg, P. O.; McElroy, C. T.; Swartz, W. H.; Kusterer, T. L.; Anderson, D. E.; Lait, L. R.; Bui, T. P. *J. Geophys. Res.* **1999**, *104*, 26687–26703.

- (25) Bradshaw, J.; Davis, D.; Crawford, J.; Chen, G.; Shetter, R.; Muller, M.; Gregory, G.; Sachse, G.; Blake, D.; Heikes, B.; Singh, H.; Mastrocinno, J.; Sandholm, S. *Geophys. Res. Lett.* **1999**, *26*, 471–474, and references therein.
- (26) Sandholm, S. T.; Bradshaw, J. D.; Dorris, K. S.; Rodgers, M. O.; Davis, D. *J. Geophys. Res.* **1990**, *95*, 10155–10161.
- (27) Wendel, G. J.; Stedman, D. H.; Cantrell, C. A. *Anal. Chem.* **1983**, *55*, 937–940.
- (28) Hesterberg, R.; Blatter, A.; Fahrni, M.; Rosset, M.; Nefel, A.; Eugster, W.; Wanner, H. *Environ. Pollut.* **1996**, *91*, 21–34.
- (29) Blanchard, P.; Shepson, P. B.; Schiff, H. I.; Drummond, J. W. *Anal. Chem.* **1993**, *65*, 2472–2477.
- (30) Chen, X. H.; Hulbert, D.; Shepson, P. B. *J. Geophys. Res.* **1998**, *103*, 25563–25568.

Although their paper did not discuss possible losses of NO<sub>2</sub> on the chromatography column, they did show losses of NO<sub>2</sub> on a variety of other common materials (e.g., aluminum and copper), suggesting an advantage for techniques with rapid flow rates and a minimum of surface contact between the instrument and the sample.

Numerous other techniques have been used in the atmosphere or suggested as new approaches—tunable infrared diode laser absorption spectroscopy (TDLAS) has demonstrated a capability for in situ detection at 400–700 ppt/10 s with approximately 100-m path lengths.<sup>32–34</sup> Detection limits using a visible diode laser and 1-m path lengths have reached 5000 ppt/10 s,<sup>35</sup> while others remain orders of magnitude higher.<sup>36,37</sup> Long-path differential absorption has been used to detect atmospheric NO<sub>2</sub> with a sensitivity of 250 ppt/10 s using a 20.6-km folded path length.<sup>18</sup> Laser imaging detecting and ranging (LIDAR)<sup>38,39</sup> and its relative, differential absorption LIDAR, have detection limits near  $2 \times 10^5$  ppt for NO<sub>2</sub>, limiting their current use to studies near the combustion sources of NO<sub>x</sub>.<sup>40</sup> Magnetic rotation spectroscopy has been used in the laboratory to achieve a detection limit of 6000 ppt/10 s.<sup>41,42</sup> The above techniques are all spectroscopically specific to NO<sub>2</sub>. However, none of them has the sensitivity of LIF.

#### LASER-INDUCED FLUORESCENCE DETECTION OF NO<sub>2</sub>

The fluorescence spectrum of NO<sub>2</sub>\* is known to be broad and unstructured except at the earliest times (single-collision conditions) following excitation. The fluorescence following laser excitation is expected to exhibit a similar wavelength distribution as the NO<sub>2</sub>\* produced by reaction of NO + O<sub>3</sub> because of the dominant role of collisional redistribution in determining energy disposal in NO<sub>2</sub>\*. An early attempt at LIF detection of NO<sub>2</sub> by Tucker et al. used a He–Cd laser with nonresonant detection and achieved a detection limit of 2040 ppt/10 s but the specificity of the approach was not commented on.<sup>43</sup> George and O'Brien used a frequency-doubled Nd<sup>3+</sup>:YAG laser with detection from 580 to 900 nm to achieve a sensitivity to NO<sub>2</sub> of 2500 ppt with 10-s averaging in a more portable configuration.<sup>44</sup> They took advantage

of the long fluorescence lifetime of NO<sub>2</sub> to discriminate against some of the resonant background scatter and used an NO<sub>2</sub> scrubbing step (reducing NO<sub>2</sub> to NO using FeSO<sub>4</sub>) to demonstrate specificity of the technique to NO<sub>2</sub>. Recently, Fong and Brune developed an LIF instrument employing a tunable dye laser as the excitation source.<sup>45</sup> They excited NO<sub>2</sub> at 564 nm with detection using a red-sensitive PMT (8% quantum efficiency) filtered to a bandwidth of approximately 200 nm. By tuning the laser on and off of a rotational resonance in the excitation spectrum, this instrument demonstrated its specificity for NO<sub>2</sub>. The sensitivity of the Fong and Brune prototype is limited by the combination of a modest signal rate (0.12 counts/10 s/ppt) and a high background count rate (approximately 10 000 counts/10 s). The reported instrument sensitivity, 1085 ppt/10 s, was about a factor of 2.5 better than that of George and O'Brien.

Perkins et al., recently designed an NO<sub>2</sub>-LIF instrument for detection of NO<sub>2</sub> aboard the ER-2 aircraft in the lower stratosphere.<sup>46</sup> The instrument, a direct predecessor to the one we describe in this article, uses a dye laser that is tuned on and off an NO<sub>2</sub> resonance near 585 nm. Detection of the total fluorescence integrated from 750 nm to the long-wavelength cutoff of a GaAs PMT occurs simultaneously with the pulsed laser. The ER-2 instrument was first demonstrated during NASA's 1997 Photochemistry of Ozone Loss in the Arctic In Summer (POLARIS) experiment. During this deployment, Perkins et al. demonstrated a detection limit of 10–50 ppt, limited by systematic noise in the background, and a sensitivity of 40–80 ppt/10 s at the ambient pressure (<200 Torr). An informal intercomparison with a PF-CL instrument showed strong correspondence between the two approaches. A linear regression of 13 075 simultaneous measurements by the two instruments obtained on 27 separate flights over a 6-month span gives [NO<sub>2</sub>]<sup>LIF</sup> = 1.07[NO<sub>2</sub>]<sup>PC</sup> and an  $R^2 = 0.95$ .<sup>24,46</sup> At pressures above 200 Torr, the ER-2 instrument's sensitivity degrades due to pressure broadening and an increase in background noise associated with 2nd Stokes Raman scattering. Nonetheless, the sensitivity of this instrument is more than a factor of 10 improvement over that of the LIF instrument designed by Fong and Brune and within a factor of that of 2 of the best PF-CL instruments. The advances we describe below improve the approach described by Perkins et al., reducing the detection limit to 1 ppt, enabling operation at any pressure within the atmosphere without loss of sensitivity, and improving the sensitivity by more than a factor of 3, to 15 ppt/10 s.

#### THE FLUORESCENCE SIGNAL

Before describing the design of our instrument, we first give some background on the expected signal rates. It is more difficult to generalize about the noise in the experiment, so that discussion is deferred to the instrument design sections where we can discuss the specific sources of noise. NO<sub>2</sub> exhibits a broad background absorption on top of which exists a complex and often congested structure from distinct molecular transitions. Since our approach to demonstrating the specificity of LIF requires the ability to tune on and off a molecular transition unique to NO<sub>2</sub>, the feature chosen for excitation is a compromise between two criteria. First, the

- (31) Gaffney, J. S.; Bornick, R. M.; Chen, Y. H.; Marley, N. A. *Atmos. Environ.* **1998**, *32*, 1445–1454.
- (32) Schiff, H. I.; Karecki, D. R.; Harris, G. W.; Hastie, D. R.; Mackay, G. I. *J. Geophys. Res.* **1990**, *95*, 10147–10153.
- (33) Webster, C. R.; May, R. D.; Allen, M.; Jaegle, L.; McCormick, M. P. *Geophys. Res. Lett.* **1994**, *21*, 53–56.
- (34) Gregory, G. L.; Hoell, J. M.; Torres, A. L.; Carroll, M. A.; Ridley, B. A.; Rodgers, M. O.; Bradshaw, J.; Sandholm, S.; Davis, D. D. *J. Geophys. Res.* **1990**, 10129–10138.
- (35) Sonnenfroh, D. M.; Allen, M. G. *Appl. Opt.* **1996**, *35*, 4053–4058.
- (36) Mihalcea, R. M.; Baer, D. S.; Hanson, R. K. *Appl. Opt.* **1996**, *35*, 4059–4064.
- (37) Gianfrani, L.; Gagliardi, G.; Pesce, G.; Sasso, A. *Appl. Phys. B* **1997**, *B64*, 487–491.
- (38) Weitkamp, C.; Goers, U. B.; Glauer, J.; Kohler, S.; Rairoux, P.; Immler, F.; Woste, L.; Ulbricht, M.; Weidauer, D. 18th International Laser Radar Conference, Berlin, Germany, 1996; Springer-Verlag; pp 411–414.
- (39) Strong, K.; Jones, R. L. *Appl. Opt.* **1995**, *34*, 6223–6235.
- (40) e.g., Toriumi, R.; Tai, H.; Takeuchi, N. *Opt. Eng.* **1996**, *35*, 2371–2375.
- (41) Blake, T. A.; Chackerian, C., Jr.; Podolske, J. R. *Appl. Opt.* **1996**, *35*, 973–985.
- (42) Smith, J. M.; Bloch, J. C.; Field, R. W.; Steinfeld, J. I. *J. Opt. Soc. Am. B* **1995**, *12*, 964–969.
- (43) Tucker, A. W.; Birnbaum, M.; Fincher, C. L. *Appl. Opt.* **1975**, *14*, 1418–1421.
- (44) George, L. A.; O'Brien, R. J. *J. Atmos. Chem.* **1991**, *12*, 195–209.

(45) Fong, C.; Brune, W. H. *Rev. Sci. Instrum.* **1997**, *68*, 4253–4262.

(46) Perkins, K. K.; Cohen, R. C.; Koch, L. C.; Stimpfle, R. M.; Lapson, L. L.; Lanzendorf, E.; Anderson, J. G. Harvard University, Cambridge, MA. Unpublished work, 1998.

signal is maximized at the wavelength where the product of the molecular fluorescence cross section and the laser intensity is largest. Second, the ability to discriminate against fluorescence from other species and other sources of noise is enhanced if the on-resonance fluorescence signal is a large multiple of the off-resonance signal. Although the absolute magnitude of both the absorption cross section and the differential absorption cross section is largest near the peak of the NO<sub>2</sub> spectrum, the ratio of resonant to nonresonant absorption (and fluorescence) has its maximum in the red region of the spectrum. In this region, the continuum absorption cross section falls off more rapidly than does the absorption due to structured features in the spectrum. As a result, our choice of excitation wavelength is a compromise between the need for sensitivity and the need for specificity. Following Perkins et al., we choose to excite NO<sub>2</sub> at 17086.5 cm<sup>-1</sup> where a pair of overlapping rotational lines (5<sub>1,4</sub> ← 4<sub>1,3</sub> and 5<sub>0,5</sub> ← 6<sub>0,6</sub>) in the (430) A<sup>2</sup>B<sub>2</sub> ← (000) X<sup>2</sup>A<sub>1</sub> vibronic band offer a contrast of roughly 3:1 (using a laser line width of 0.06 cm<sup>-1</sup>) between the online and offline signals.<sup>46</sup> The peak absorption cross section is 1 × 10<sup>-19</sup> cm<sup>2</sup>/molecule.<sup>47</sup>

The fluorescence signal scales linearly with excitation rate, fluorescence efficiency, and the signal-collection efficiency. The excitation rate, in units of NO<sub>2</sub> molecules excited per second, can be expressed as

$$\text{Excitation Rate} = [\text{NO}_2]l \int \Phi(\nu, \nu_{\text{laser}}) \sigma(P, T; \nu, \nu_0) d\nu \quad (1)$$

where [NO<sub>2</sub>] is the number density of NO<sub>2</sub> (molecules/cm<sup>3</sup>), *l* is the path length (cm) imaged onto the detector, and the integral represents the overlap of the laser line shape, Φ(ν, ν<sub>laser</sub>) (photons/s), with the molecular line shape, σ(P, T, ν, ν<sub>0</sub>) (cm<sup>2</sup>/molecule). The molecular line width is subject to pressure and Doppler broadening, and the absorption cross section depends on the thermal population of the initial rotational states. Assuming a Gaussian laser line shape and molecular line shape, the overlap integral becomes

$$\int \Phi(\nu, \nu_{\text{laser}}) \sigma(P, T; \nu, \nu_0) d\nu = F \sigma_{\text{pk}} \left[ \frac{\Delta \nu_{\text{D}}^2}{\Delta \nu_{\text{L}}^2 + \Delta \nu_{\text{D}}^2} \right]^{1/2} \quad (2)$$

where *F* is the integrated laser intensity (photons s<sup>-1</sup>), σ<sub>pk</sub> is the absorption cross section at the peak (cm<sup>2</sup>), and Δν<sub>D</sub><sup>2</sup> and Δν<sub>L</sub><sup>2</sup> are the full widths at half-maximums of the molecular (Doppler) and laser line shapes, respectively. Note that this useful approximation is not as accurate as it often is because the NO<sub>2</sub> absorption resonances are embedded in a broad continuum.

The fraction of excited NO<sub>2</sub> molecules that fluoresce is governed by the competition between radiative and collisional relaxation:

$$\text{Fluorescence Efficiency} = \frac{k_r}{k_r + \sum_i k_{\text{qi}} [M_i]} \quad (3)$$

Measurements of fluorescence lifetimes and fluorescence quenching rates for NO<sub>2</sub> depend strongly on the bandwidth of

the excitation laser and detection system. The radiative decay is slow (*k<sub>r</sub>* ~ 10 000 s<sup>-1</sup>) and the collisional relaxation rapid (*k<sub>qi</sub>* ~ 6 × 10<sup>-11</sup> cm<sup>3</sup>/molecules/s). As a result, the fluorescence quenching rate, Σ *k<sub>qi</sub>* [M<sub>*i*</sub>], is large compared with the radiative rate, *k<sub>r</sub>*, at all pressures greater than 0.1 Torr.<sup>48</sup> The NO<sub>2</sub> fluorescence efficiency in an atmospheric sample simplifies to

$$\text{Fluorescence Efficiency} \cong \frac{1}{Q[M]} \quad (4)$$

where *Q* is a temperature- and composition-dependent quenching factor specific to a particular experimental situation (excitation and detection bandwidths) and [M] is the total number density (molecules/cm<sup>3</sup>). Observations by Mazely et al. and Patten et al. suggest a stepwise mechanism for vibrational de-excitation of NO<sub>2</sub> that qualitatively explains the long fluorescence lifetime and rapid collisional effects.<sup>49,50</sup> However, no measurements exist that allow one to accurately predict the fluorescence lifetime or quenching rate for an experiment with arbitrary choices of excitation and detection bandwidths. The quenching of NO<sub>2</sub> fluorescence by H<sub>2</sub>O has been measured to be about 6 times faster (at similar but not identical wavelengths) than that by N<sub>2</sub> or O<sub>2</sub>.<sup>51</sup> As a result, the quenching factor for an atmospheric sample can vary by as much as 20% between the highest and lowest possible absolute humidity (0–20 Torr of water vapor), and so accurate measurements of NO<sub>2</sub> in the lower atmosphere require simultaneous observations of absolute humidity. Finally, it is useful to notice that at pressures above 0.1 Torr, the [NO<sub>2</sub>] term in the excitation rate, (eq 1), combines with the [M]<sup>-1</sup> term in the fluorescence efficiency equation, (4), to make the signal count rate directly proportional to the NO<sub>2</sub> mixing ratio not to its absolute number density.

The collection efficiency is the fraction of fluorescence that is detected by the PMT, and it depends on the following instrumental parameters:

$$\text{Collection Efficiency} = \Omega \int T(\nu) \eta(\nu) \epsilon(\nu) d\nu \quad (5)$$

Ω is the fraction of the solid angle intercepted by the detection apparatus, and the integrand is a product of the transmission function of the collection optics, *T*(ν), the quantum efficiency of the PMT, η(ν), and, ε(ν), the fraction of the total fluorescence occurring within the band-pass of the PMT. The signal count rate for the LIF instrument is given by a product of eqs 1, 3, and 5, i.e.:

$$S_{\text{NO}_2} = \text{Excitation Rate} \times \text{Fluorescence Efficiency} \times \text{Collection Efficiency} \quad (6)$$

For 100 mW of laser power and 1 ppt of NO<sub>2</sub> at a total pressure of 3.5 Torr, the excitation rate is approximately 6.6 × 10<sup>4</sup> NO<sub>2</sub>\*.

(47) Burrows, J. P.; Dehn, A.; Deters, B.; Himmelmann, S.; Richter, A.; Voigt, S.; Orphal, J. *J. Quant. Spectrosc. Radiat. Transfer* **1998**, *60*, 1025–1031.

(48) Donnelly, V. M.; Kaufman, F. *J. Chem. Phys.* **1978**, *69*, 1456–1460.

(49) Mazely, T. L.; Friedl, R. R.; Sander, S. P. *J. Chem. Phys.* **1994**, *100*, 8040–8046.

(50) Patten, K. O., Jr.; Burley, J. D.; Johnston, H. S. *J. Phys. Chem.* **1990**, *94*, 7690–7699.

(51) Donnelly, V. M.; Keil, D. G.; Kaufman, F. *J. Chem. Phys.* **1979**, *71*, 659, 673.

s<sup>-1</sup>. The fluorescence efficiency at 3.5 Torr is on the order of  $5.6 \times 10^{-3}$ ,<sup>52</sup> and the collection efficiency of our experimental set up is approximately  $1.5 \times 10^{-4}$ . An online signal count rate of  $5.5 \times 10^{-4}$  counts/s/ppt/mW is expected. This count rate is approximately a factor of 5 greater than that reported by Fong and Brune,<sup>45</sup> and slightly less than that reported by Perkins et al. of  $7.0 \times 10^{-4}$  counts/s/ppt/mW.<sup>46</sup>

## EXPERIMENTAL SECTION

In addition to having a high signal count rate and a low detection limit, an atmospheric measurement system must be calibrated precisely to be useful. If the goal is to observe trends, as we hope to do in the future, then diagnostics and procedures that maintain and demonstrate that the calibration is precise to better than 1% per year must be integral to the LIF instrument design. We use the following model to describe instrument calibration and to illustrate issues related to precision of the calibration on different time scales:

$$[\text{NO}_2]_{\text{measured}} = C(t)[\text{NO}_2]_{\text{true}} + \text{zero}(t) \quad (7)$$

and

$$C(t) = C_0 C(\text{adjustments}) C'(\text{drift}) C''(\text{random}) \quad (8)$$

The measured value of NO<sub>2</sub> is equal to the true NO<sub>2</sub> when  $C(t)$  is equal to 1 and  $\text{Zero}(t)$  is equal to zero. The temporal dependence of  $C(t)$  is divided into four parts: (i)  $C_0$ , represents the time-invariant calibration. Uncertainties in this term include the temperature dependence of the NO<sub>2</sub> fluorescence signal, the concentration of the calibration standard, and related factors that could be better determined by laboratory experiments. (ii)  $C''$  (random) represents the finite precision of the instrument. Averaging any subset of measurements will improve the precision of the measured concentration by bringing  $C''$  (random) closer to a value of 1. The other components of the calibration represent factors that are time-varying that must be tracked in the field during the course of every measurement campaign. (iii)  $C'$  (drift) describes factors that vary slowly and continuously such as might occur if the laser alignment or transmission band-pass of the optical filters used were slowly degrading or the concentration of the calibration standard were changing. (iv)  $C$  (adjustments) describes systematic changes to the instrument that result from operator intervention. These sorts of adjustments to the instrument might result in systematic offsets between the instrument calibration for different measurement periods if they are not properly tracked. The effects of operator adjustments may average away if observations taken with many different adjustments can be combined. However, this is not usually the case. We have confidence in trends measured by an instrument when the time-dependent components of the calibration are all equal to 1 and NO<sub>2</sub> is large compared to the uncertainty in the instrument zero. This confidence holds even if there is a large uncertainty in the time-independent calibration constant  $C_0$  and individual measurements have a large random uncertainty. In the sections below, we detail the design of the LIF instrument with attention to the

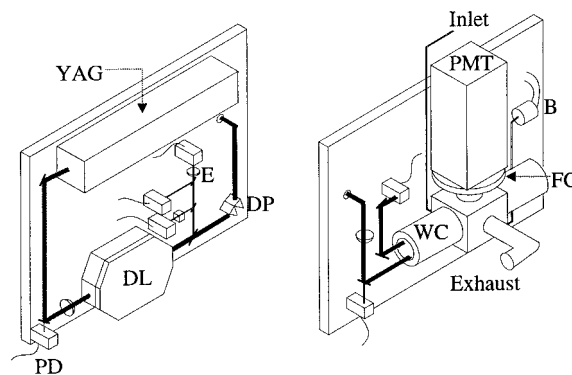


Figure 1. Schematic of the UC, Berkeley laser-induced fluorescence (LIF) NO<sub>2</sub> instrument. The core of the instrument is mounted on a breadboard, one side holding the laser subsystem and the other side the detection axis. A frequency doubled Nd<sup>3+</sup>:YAG laser (YAG) at 532 nm pumps a custom-built dye laser (DL), the output (585 nm) of which is sampled by fused silica beam splitters to monitor power, frequency (by measuring transmittance through an NO<sub>2</sub> reference cell shown as a cube), and line width measured with an external etalon (E). Six photodiode detectors (PD) are used to measure laser power at various points along the beam path. A set of dispersion prisms (DP) is used to separate the 585 nm light from the 532 nm light which is then dumped. The 585 nm light is then sent through a hole in the breadboard to the detection side to the multipass White Cell (WC). The pressure in the WC is measured with a manometer, 100 Torr Baratron (B). NO<sub>2</sub> fluorescence is collected and sent through a series of optical filters housed in the filter changer (FC) to the photomultiplier tube in its TE-cooled housing (PMT).

factors that control sensitivity, accuracy, and stability of the calibration over time.

The Berkeley NO<sub>2</sub> instrument can be divided into four major subsystems: (a) excitation laser, (b) detection cell, (c) gas flow and handling, and (d) data acquisition and instrument control. Figure 1 is a schematic of the laser and detection assemblies. The majority of the instrument is packaged in a standard (19") equipment rack that is  $1.4 \times 0.5 \times 0.75$  m in size. The entire instrument occupies about 1 m<sup>3</sup> and weighs 200 kg. The 19" rack contains the laser and laser power supply, the detection assembly, gated photon-counting electronics, and mass-flow controllers used for addition of calibration gases. Additional separate components include the dye recirculation system, a closed cycle liquid loop maintained at 20 °C, a vacuum pump, calibration gases, and the data acquisition and control computer.

**a. Laser Subsystem.** The laser and detection subsystems are mounted on opposite sides of a standard aluminum breadboard ( $60 \times 45 \times 2$  cm). The assembly is sealed against drafts and dust with a sheet metal cover that also serves to eliminate the eye hazard associated with a high-power visible laser. A compact, diode-pumped, Q-switched, frequency-doubled Nd<sup>3+</sup>: YAG laser (T40-X30, Spectra Physics, average power of 3 W at 532 nm, 30-ns pulse length) pumps a tunable dye laser at 8 kHz. The beam is focused into a homebuilt Etalon-tuned dye laser of a design described by Wallace and as repackaged by Wennberg et al. for detection of stratospheric OH by LIF at 282 nm.<sup>53</sup> The dye laser is operated on the laser fundamental (585 nm), eliminating the need for a doubling crystal, but the high gain of the laser without

(53) Wennberg, P. O.; Cohen, R. C.; Hazen, N. L.; Lapson, L. B.; Allen, N. T.; Hanisco, T. F.; Oliver, J. F.; Lanham, N. W.; Demusz, J. N.; Anderson, J. G. *Rev. Sci. Instrum.* **1994**, *65*, 1858–1876, and references therein.

(52) Larabee, J. K. Ph.D. Thesis, Harvard University, Cambridge, MA, 1984.

this crystal required replacing the tuning mirror with an 1800 grooves/mm holographic grating to suppress higher order laser modes. The dye laser is contained in a pressure housing capable of sustaining 100 Torr differential pressures for months. Its temperature is stabilized at  $36 \pm 0.5$  °C using high temperature coefficient of resistance heaters as both the heat source and temperature sensor (Minco part no. HK20323). The dye laser emits 25-ns (fwhm) pulses with a line width of approximately  $0.06 \text{ cm}^{-1}$  at 585 nm.

We use a dye solution of Kiton Red (0.2 g/L) in an Ammonyx (Exciton): water (3:97) mixture. The solution is pumped through the dye cell at approximately 1 L per minute. Teflon and stainless steel plumbing is used throughout the dye system to minimize chemical degradation of the dye. Both the dye reservoir and the  $\text{Nd}^{3+}$ : YAG laser head are actively cooled with a recirculating water loop which is, in turn, maintained near room temperature with a small radiator. We chose the Kiton Red dye solution despite its modest output power (typically, 100 mW) because of its exceptionally long lifetime. In a system with a dye reservoir of 1 L, we have used it continuously (24 h a day, 7 days a week) for periods exceeding two weeks without loss of laser power. In contrast, Pyrromethene 597 (in 2-propanol) is much more efficient, peak powers observed in the laboratory are 400 mW at 585 nm, but the laser power observed using this dye decays on a time scale of days. Furthermore, the dye frequently burns onto the dye cell windows causing sudden and complete loss of laser emission.

The output from the dye laser is collimated and directed through a pair of equilateral SF10 quartz prisms to separate the 532-nm pump beam from the 585-nm beam. The 585-nm beam is then sent through the breadboard to the detection cell. Along the way, a small fraction of the beam is sampled using uncoated 45° quartz beam splitters and directed onto separate photodiodes that track laser power, laser frequency, and the laser line width. A similar diode is used to monitor the power of the YAG laser using the light that leaks through a 99% reflective 45° turning mirror as the signal. The laser frequency is monitored by measuring the transmittance through a 2.5-cm reference cell filled with 20 Torr of pure  $\text{NO}_2$ . Comparison of reference spectra recorded in the laboratory and the atlas compiled by Hsu et al.,<sup>54</sup> is sufficient to confirm the laser wavelength. The laser line width is determined by analysis of the transmission of the beam through an external high-finesse ( $>60$ ) Etalon (free spectral range of  $0.54 \text{ cm}^{-1}$ ) during scans of the laser wavelength.

**b. Detection Cell.** The detection cell, see schematic in Figure 2, is built around a 40-pass, 30.5-cm White cell with the design goal of maximizing the  $\text{NO}_2$  fluorescence collected while minimizing collection of scattered light from other sources. The polarized laser beam propagates through this cell with the  $E$  vector parallel to the detector. Fluorescence is collected from a volume that is 1 cm on the long axis of the White cell and approximately  $2 \times 20$  mm in cross section. The fluorescence is collected using a 32-mm-diameter, 38-mm focal length lens (L1) and a retroreflecting mirror (M4) with a radius of curvature of 44 mm located opposite the collection lens. These optics intercept roughly 5% of the solid angle for a point at the center of the cell. The extended source

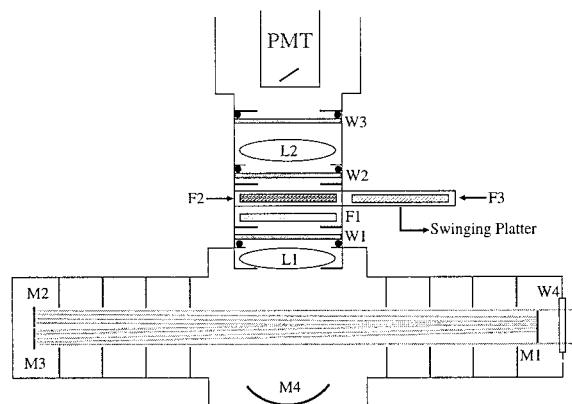


Figure 2. Schematic of the detection axis. White Cell mirrors (M1–M3) are separated by their radii of curvature, 30.5 cm. A spherical mirror (M4, radius of curvature 44 mm) is used to double the fraction of the solid angle collected. The limiting aperture to the optical train located in front of the first lens, L1, is 32 mm. The collection lens (L1), with a 50-mm focal length, collimates light through the dielectric filters (F1–F3). Light is focused by a 75-mm focal length lens L2 onto the PMT. F1 is a 610-nm-long pass (LP) filter. F2 is a 700-nm LP filter used during  $\text{NO}_2$  detection, and F3 is a narrow bandwidth ( $<15$  nm fwhm) filter centered at 676 nm for monitoring  $\text{N}_2$ -Raman scatter. F2 and F3 are exchanged by moving the swinging platter back and forth. W1–W4 are windows; W2 and W3 seal the cooled PMT ( $\sim -25$  °C).

region makes it difficult to optimize the collection efficiency. However, alternative strategies for directing the laser fluence to a single point for improved image quality on the photocathode (e.g., a Herriot Cell<sup>55</sup>) require focusing the laser in the center of the cell with consequent saturation of the  $\text{NO}_2$  optical transition. Saturation reduces the optical sensitivity as well as our ability to measure the noise and, per unit laser power, our ability to use on/off resonance signals to ensure specificity.

After collection by the lens, L1, the light passes through a series of optical filters to reject light from sources other than  $\text{NO}_2$  fluorescence. We attempt to strongly discriminate against: (1) light from sources that are spatially coincident with, but at different wavelengths from, the  $\text{NO}_2$  fluorescence including Rayleigh and Raman scatter, and (2) scatter that is not spatially coincident with the  $\text{NO}_2$  fluorescence but is at the same wavelengths such as the broadband fluorescence generated on surfaces of the optics and detection chamber. We expect on of order  $10^8$  Rayleigh photons per second setting a minimum level of blocking required at 585 nm.

A 610 nm dielectric long pass filter (Omega Optical, Inc) with extra blocking at 585 nm provides high transmission ( $>80\%$ ) of light with wavelengths longer than 650 nm with at least  $10^{-5}$  attenuation at 585 nm and good rejection of any residual 532-nm light. A 700-nm dielectric long pass filter directly follows the 610 nm long pass filter to block Raman scattering of the laser light by  $\text{N}_2$  and  $\text{O}_2$ . This second filter strongly rejects wavelengths less than 700 nm ( $10^{-5}$  attenuation for wavelengths between 585 and 680 nm) and transmits greater than 80% for wavelengths greater than 750 nm. The attenuation provided by these filters is sufficient to reduce any pressure-dependent scatter (Rayleigh scatter and Raman scatter) to below our detection limit. For calibration purposes, the  $\text{NO}_2$  filter is occasionally replaced with a filter that

(54) Hsu, D. K.; Monts, D. L.; Zare, R. N. *Spectral Atlas of Nitrogen Dioxide 5530 to 6480 Angstroms*; Academic Press: New York, 1978.

(55) Herriott, D. R.; Kogelnik, H.; Kompfner, R. *Appl. Opt.* **1964**, *3*, 523–526.

transmits at 670 nm ( $676 \pm 8$  nm) for detection of  $N_2$  Raman. The 700-nm LP ( $NO_2$  detection mode) and the 676 nm band-pass ( $N_2$ -Raman mode) filters are mounted on a motorized swinging platter which, under computer control, rotates the desired filter in and out of the optical path within one second. The swinging platter is temperature controlled to prevent changes in filter transmission, and it is enclosed in a light-sealed aluminum housing. The band-pass filter is used to transmit light from the  $N_2$ -Raman transition (greater than 80% transmission between 674 and 680 nm), while attenuating light outside this region by  $10^{-5}$ . The light transmitted by the filters is focused ( $L_2$ , 75 mm) onto the cooled ( $-20$  °C) 10 mm  $\times$  4 mm GaAs photocathode (C31034A, Burle Technologies). Pulses from the PMT are sent through an AC-coupled preamplifier and are then counted by a two-channel gated photon counter (SR400, Stanford Research Systems). We calculate the transmission through the optical train to the PMT to be 50% from 700 to 1000 nm. The lenses and two windows used to thermally isolate the photocathode are not A/R coated in this current system. A/R coating could increase the transmission to 64%.

With the optical filters in place, the majority of the noise in the instrument originates at the White cell mirrors, where light that is not reflected ( $<0.1\%$  per pass) but is partially red-shifted and re-emitted isotropically. We use series of baffles to eliminate the view of the bright White cell optics by the collection lens and the retroreflector. These baffles and the walls of the detection cell are coated with a low fluorescence optical black paint (MH2200, IIT Research Institute) to reduce the scattering of stray light off of their surfaces. To further reduce the unwanted laser scatter, we use a time gated photon counting technique similar to that described by George and O'Brien<sup>44</sup> to separate the scatter and any short-lived fluorescence from the long-lived  $NO_2$  fluorescence. The technique relies on holding the sample pressure constant in the range of 2–4 Torr.

The advantages of the delayed gate approach include the noise reduction and the elimination of pressure broadening. Both are essential to operation at the Earth's surface. The disadvantages of the delayed gate approach are the need for a vacuum pump, which substantially raises the weight and power of the experiment, and the potential for additional imprecision and systematic error introduced into the measurement by collecting only a fraction of the  $NO_2$  fluorescence. As we discuss later, these potential systematic errors are quite small ( $<3\%$ ), and we describe strategies for reducing them further. Figure 3 shows the fluorescence signal from  $NO_2$  at 2 Torr total pressure, as well as the background noise (no  $NO_2$  present) versus the time delay from the moment the laser enters the White cell. As can be seen in the figure, the majority of the background noise occurs during the 40-ns transit time of the laser pulse in the cell. After 55 ns, the background noise has dropped by several e-folds but the  $NO_2$  fluorescence signal decays with a lifetime of approximately 270 ns. Delaying photon counting until 55 ns gives a 95% reduction in background noise, while collecting roughly 85% of the  $NO_2$  fluorescence signal. Following initial field tests in 1998, we have operated at 3.5 Torr. At this pressure we can use narrower gates due to the shorter fluorescence lifetime ( $\sim 150$  ns) suppressing thermal noise while still collecting about 82% of the fluorescence signal.

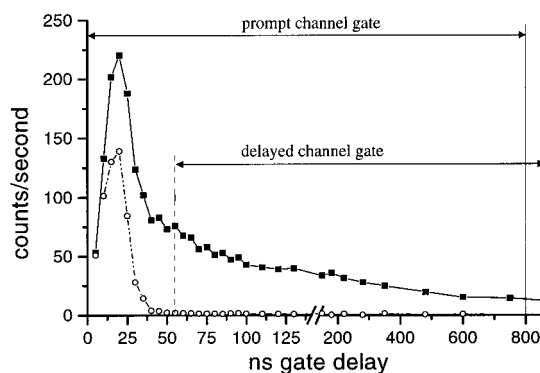


Figure 3. Total signal for 50 ppbv  $NO_2$  (squares) and 0 ppbv  $NO_2$  (circles), i.e., background signal, at 2 Torr are plotted versus delay from when the laser pulse enters the detection cell. The points represent 1-second integrations of 10-ns-wide gates at 8 kHz. One channel of the counter has a zero-delayed, 800-ns-wide gate to catch all signal prompt with the laser pulse. The other channel has a 55-ns-delayed, 800-ns-wide gate to eliminate scatter prompt with the laser pulse. The area under the fluorescence curve remains large ( $\sim 75\%$ ) in the delayed gate, while the background noise has essentially decayed to zero.

With the delayed gate approach, we have achieved a background count rate of  $1.5$  counts  $s^{-1}$  at 100 mW of laser power. Of this,  $1.2$  counts  $s^{-1}$  are laser-induced. We use 750-ns-long gates and operated at 8 kHz, so the experimental duty cycle is 0.6%. Therefore, the PMT dark count rate of approximately  $50$   $s^{-1}$  contributes  $0.3$  counts  $s^{-1}$  to the background. A 30-s integration of the laser-induced background is precise to 4 ppt ( $1\sigma$ , 100 mW). On the basis of longer averages, we have no evidence that there exist systematic errors in the background greater than 1 ppt.

**c. Sampling.** We sample through a stainless steel pinhole held in a steel ultraTorr fitting. Air is pumped through a 10 m long, 6 mm i.d. PFA tubing into the detection cell using a 10 cfm rotary vane pump. The pressure in the cell is held constant, most often at  $3.5$  ( $\pm 0.1$ ) Torr and is monitored with a 100 Torr stainless steel capacitance manometer (MKS Part no. 626, 100 Torr). Wall effects are minimized by keeping the detection cell small, about one liter. Rapid air flow (1500 sccm) results in a residence time in the tubing and the cell of approximately 1 s. To produce good instrument zeros, we constantly purge the end caps of the White Cell which contain the mirrors (M1–M3) with zero air at 1% of the total flow. We also regularly purge the plumbing from the regulator on the  $NO_2$  cylinder through the flow controller to the cell.

The rapid response time of the instrument is illustrated by the data shown in Figure 4. The figure shows a period with short  $NO_2$  plumes from an unidentified source (most likely a delivery truck) wafting across our inlet. The  $NO_2$  mixing ratio increases by 2 orders of magnitude in less than 5 s as the plume crosses the inlet. The rapid recovery of the system back to ambient background concentrations (about 4 ppb) within 5 s shows that the instrument is free from memory effects associated with this short pulse of  $NO_2$  absorbing and then desorbing from the tubing walls. Analysis of the calibration data shows that from the end of the last nonzero flow (3–4 ppb) to the end of the zero measurement there exists a small tail in the signal as it approaches the background count rate. This suggests that there are some wall effects in our system producing a desorption limited rate of 10–20 s for the system to go from 300 ppb to the true zero.

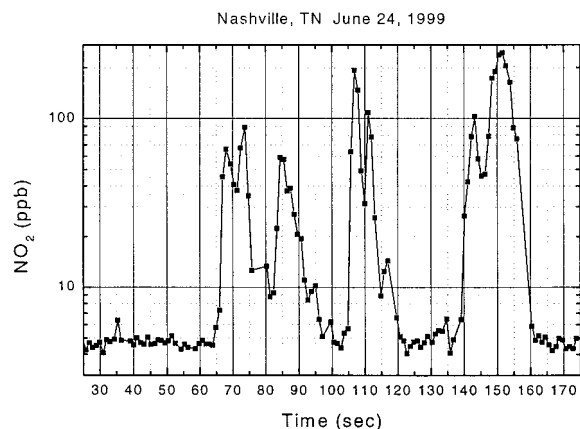


Figure 4.  $\text{NO}_2$  during a plume from an unidentified source at Cornelia Fort Airpark in Nashville, TN. 1 Hz data are plotted vs time in seconds and are from June 24, 1999 at approximately 4:15 PM Central Standard time. Background concentrations of  $\text{NO}_2$  were near 4 ppb during this period.

**d. Calibration.** Our model of instrument performance, eqs 7 and 8, guides our design of a calibration system. Parameters describing the base calibration of the LIF technique ( $C_0$  in eq 8) were determined by measuring the instrument response to a series of  $\text{NO}_2$  standards. Mixing ratios in the range 500 ppt–50 ppb were prepared by dynamic dilution of 3 separate certified standards of  $\text{NO}_2$ : 5.08 ( $\pm 0.10$ ) ppm, 49.9 ( $\pm 1.0$ ) ppm, and 0.599 ( $\pm 0.012$ ) ppm, with the accuracy reported by the manufacturer, Scott Specialty Gases. The calibrations from these standards were self-consistent to  $\pm 5\%$ . The flows were also split and measured simultaneously by the LIF instrument and a commercial  $\text{NO}_2$  chemiluminescence instrument (TECO 42CY) calibrated with a separate certified  $\text{NO}$  standard (Scott Specialty Gases). The two instruments agreed to better than 5%.

The reference point chosen for the calibration is  $\text{NO}_2$  in dry air, at 298 K and 3.5 Torr, with a 750-nm wide gate delayed by 55 ns from the time the pulse enters the detection cell. Our expectation is that the ratio of instrument sensitivity, at a fixed pressure, gate width and delay, temperature, and absolute humidity, to  $\text{NO}_2$  and to its sensitivity to the prompt Raman scattering off of  $\text{N}_2$  is a time-invariant property of the filters/PMT combination. We then determine other constants describing the change in the calibration under other conditions (e.g., high humidity, different pressures, temperatures, or gate delay).

The time variance of the calibration is measured using 3 different approaches to ensure high precision and to investigate the accuracy of each method.

(1) We measure the sensitivity  $\text{N}_2$ -Raman scatter every 20 min. During the  $\text{N}_2$ -Raman detection mode, a narrow band-pass (<15-nm fwhm) filter, centered at 676 nm, replaces the 700-nm LP filter in the  $\text{NO}_2$  configuration and zero air is flowed into the detection chamber at various rates to observe the number density dependence of the Raman signal. Because  $\text{NO}_2$  fluorescence will leak through the band-pass filter (as much as 10%), zero air is required for precise Raman measurements in an urban environment where the  $\text{NO}_2$  signal is large and changing rapidly. We then use the measured Raman sensitivity vectors to normalize away changes in laser alignment and optical throughput from the signal.

(2) We perform calibrations in dry air every 3 h. A cylinder of zero air and a cylinder of 5.08  $\pm$  0.10 ppm  $\text{NO}_2$  in  $\text{N}_2$  (Scott

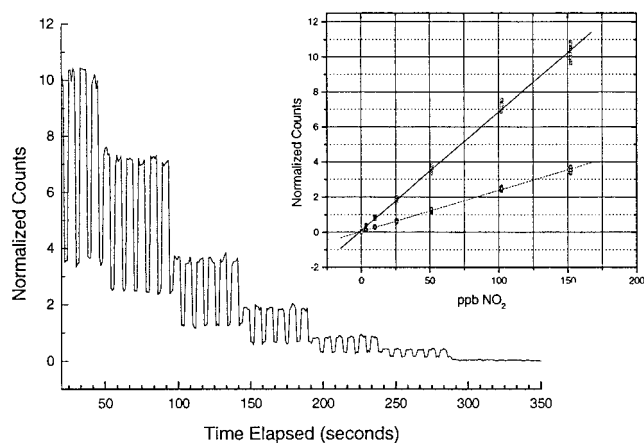


Figure 5. Calibration to  $\text{NO}_2$  during deployment at Blodgett Forest. Concentrations ranging from 150 to 0 ppb are stepped through, and the fluorescence is measured while tuning the laser frequency on and off the rovibronic transition. The photon counts are normalized to laser power and to  $\text{N}_2$ -Raman scatter in the chamber, and backgrounds are subtracted. The inset shows the resulting calibration plot for both online (squares) and offline (circles) counts, which demonstrate a constant online–offline ratio of  $\sim 3:1$

Specialty Gases with ACULIFE coating) are used for dynamic dilution from 2.5 to 150 ppb. Two mass-flow controllers are used to obtain the desired concentration range (MKS Part no. 1179A, 5000 sccm full scale for the air and 20 sccm full scale for the  $\text{NO}_2$  mixture). An additional solenoid valve directly following the  $\text{NO}_2$  flow controller provides a hard zero for the calibrations and prevents contamination of the sample flow. A three-way valve switches the flow between the sample line and the dry air calibration system. Just prior to the calibration, the zero air flow is adjusted to match the cell pressure to that of the atmospheric sample. A series of preset  $\text{NO}_2$  flow rates are used, from high to low (Figure 5).

(3) We perform standard additions to an atmospheric sample every 15 h. During a standard addition,  $\text{NO}_2$  is added to the atmospheric sample stream just prior to the detection cell (after the pressure drop of the pinhole and flow controllers). The same  $\text{NO}_2$  flows are stepped through as those during a zero-air calibration.

All evidence collected to date supports the idea that the  $\text{N}_2$  Raman calibration is an extremely precise transfer standard of instrument sensitivity. With the exception of the first 2 days of the field campaign in Nashville, TN, the minimum to maximum variation of the Raman sensitivity was 7% with a signal count rate of 4.4 counts/s/Torr/mW over the remaining 27 days. Moreover, the short-term precision, as judged by the difference in adjacent measurements of the sensitivity, is better than 0.5%. If the  $\text{N}_2$  Raman calibration is a precise transfer of changes in optical throughput and laser alignment, then the ratio of the  $\text{NO}_2$  sensitivity to the  $\text{N}_2$ -Raman sensitivity should be a constant. Observations of this ratio obtained from the Nashville campaign show that it varied by less than  $\pm 3.5\%$  ( $2\sigma$ ) whereas the unnormalized  $\text{NO}_2$  alone varied by  $\pm 5\%$  ( $2\sigma$ ).

The observed count rate is converted to  $\text{NO}_2$  mixing ratios using the measured calibration constant. The counts are normalized to laser power accounting for any short-term fluctuations in sensitivity. Laser power varies 5–50% on the time scales of seconds to days. We calculate a running mean of the  $\text{N}_2$ -Raman sensitivity

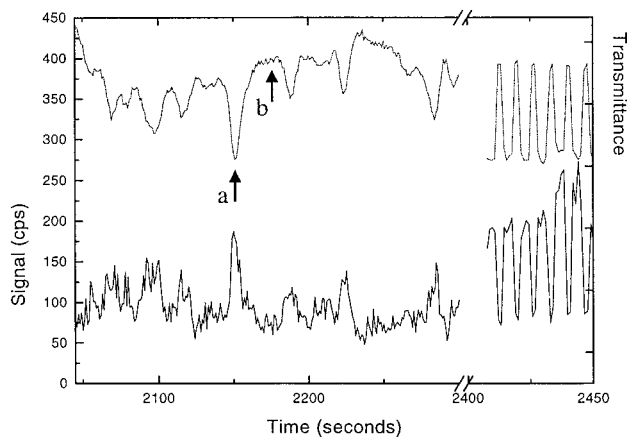


Figure 6. Scanning and dithering. In the plot, signal counts per second of laboratory air are plotted versus time during a scan of the laser frequency followed by dithering, i.e., tuning the laser on and off the molecular transition. Transmittance through the NO<sub>2</sub> reference cell during this period is plotted on the right axis. The arrows indicate the online (a) and offline (b) positions for our rovibronic feature. The NO<sub>2</sub> concentration in the laboratory was increasing during the dithering period.

from our checks in the N<sub>2</sub>-Raman monitoring mode and normalize the counts to this running mean to account for slow variations in optical throughput. Changes in laser alignment or optical throughput seem to be related to thermal drift and can lead to as much as a 15% change in sensitivity. While dithering on and off the NO<sub>2</sub> line, the etalon drive, at times, takes too many or too few steps, which results in an overshooting or undershooting, respectively, of the frequency of the peak leading to a lowering of instantaneous sensitivity. We correct this by monitoring the absorbance through our reference cell. Using the absorbance, we calculate the deviation from the true on-line position and scale the on-line counts accordingly. The size of this correction is 3–5% on average. Accounting for these changes in sensitivity ensures that the limit to the instrument's precision is that determined by photon counting statistics. Finally, we correct for changes in the absolute humidity of the atmospheric sample which can lead to as much as 10% changes in sensitivity.

**e. Data Acquisition and Control.** The data acquisition system runs under LabVIEW (National Instruments), a graphical programming language designed for multitasking instrument control and data collection. The LIF instrument is designed to be completely autonomous. The control system turns on automatically after booting Windows '95, scans the laser frequency, identifies and locks onto the NO<sub>2</sub> absorption line, and then tunes on and off this line while logging photon counts and other information. The system also schedules and performs standard addition and dry-air calibrations, frequency scans, and N<sub>2</sub>-Raman measurements. Data required to calculate NO<sub>2</sub> mixing ratios are recorded at 1 Hz, and other diagnostics are recorded at lower rates. A total of 16 A/D channels are used.

**Sensitivity and Interferences.** Figure 6 shows the basic operation involved in obtaining measurements of NO<sub>2</sub>. First, the laser frequency is scanned and the measured transmission through the NO<sub>2</sub> reference cell is compared to a stored spectrum. The frequency is then tuned to that of the chosen molecular transition, and the difference of the fluorescence on and off the line achieved by tuning the laser on and off this transition gives

a signal that is proportional to NO<sub>2</sub>. If the background is known or zero, the online and offline signals may be used individually to retrieve NO<sub>2</sub> mixing ratios from the fluorescent count rate. In practice, the online signal is the primary signal and we use the offline signal as a check against interferences. We check for interferences by using the measured online signal and the online-to-offline ratio (measured by calibrations and with the NO<sub>2</sub> reference cell) to calculate the appropriate offline signal. If the calculated offline signal equals the measured offline signal then there are no interferences. To date, we have found no evidence for chemical interferences. Particles at concentrations normally found in the polluted atmosphere have no effect on our signal; however, we have not tested the instrument in stacks or over fires where large particles exist in very high concentrations. The signal-to-noise ratio for the online signal is:

$$\frac{S}{N} = \frac{S_{\text{online}}}{\sqrt{S_{\text{online}} + B}} \quad (9)$$

At 100 mW of laser power, the online signal count rate is 600 counts/ppb/10 s and the laser induced background count rate is 12.0 counts/10 s. The detection limit for our prototype instrument is 15 ppt/10 s (signal-to-noise of 2).

**Accuracy and Precision.** The largest uncertainty in a reported NO<sub>2</sub> mixing ratio arises from the uncertainty in the concentration of the calibration standard. As discussed above, we attempt to minimize this uncertainty by comparing several standards and by comparing the LIF instrument to an NO<sub>2</sub> chemiluminescence instrument that is calibrated with an independent NO standard. We believe the concentrations of our calibration standards are accurate to 5%. The accuracy of the NO<sub>2</sub> mixing ratio recorded by our LIF instrument is also affected by our knowledge of three other factors: (1) atmospheric water vapor's influence on the fluorescence quenching, (2) the effect of pressure and/or the timing of the delayed gate on the fraction of fluorescence collected, (3) the effect of changes in the excitation rate as a result of changes in overlap of the laser and molecular line widths and in the ground-state population due to temperature changes.

Using quenching rate constants for the continuum fluorescence measured by Donnelly et al.,<sup>51</sup> we calculate a fluorescence quenching rate for NO<sub>2</sub> in zero air, which contains primarily N<sub>2</sub> and O<sub>2</sub>, with less than 5 ppm H<sub>2</sub>O and 1 ppm CO<sub>2</sub>, to be  $3.79 \times 10^6 \text{ s}^{-1}$  at 2 Torr. This rate yields a fluorescence lifetime of 263 ns at 2 Torr, which compares well with the 270-ns lifetime we measure experimentally. Again using the quenching rates observed by Donnelly et al., for a mixture of 1.25% water, 1% argon, 360 ppm CO<sub>2</sub>, 20% O<sub>2</sub>, and 77.8% N<sub>2</sub>, we calculate a quenching rate of  $4.03 \times 10^6 \text{ s}^{-1}$  at 2 Torr. This rate yields a fluorescence lifetime for NO<sub>2</sub> of 248 ns, 5.7% lower than that calculated for a zero air mixture. This difference is consistent with the observations of a 4–6% lower sensitivity to NO<sub>2</sub> in ambient air at Blodgett Forest (average absolute humidity, ~1.25%) than in dry air. The lowered sensitivity is due to the increased fluorescence quenching rates in atmospheric air relative to those in zero air. We estimate, on the basis of observations from Blodgett Forest and Nashville, TN, that quenching of the NO<sub>2</sub> fluorescence by water vapor is 4.5 (±1) times faster than that of N<sub>2</sub> or O<sub>2</sub>. Thus NO<sub>2</sub> mixing ratios

calculated from zero air calibration constants must be corrected by 3.5 ( $\pm 1$ )% per 1% change in the absolute humidity (i.e., 0.01 change in the atmospheric water mole fraction). Although Donnelly et al. estimate the fluorescence quenching by CO<sub>2</sub> to be twice as fast as that by N<sub>2</sub> or O<sub>2</sub>, atmospheric CO<sub>2</sub> does not vary enough to affect the calculated NO<sub>2</sub> concentration on the percent level. The uncertainty in the quenching rate by water vapor results in an uncertainty of the order of 2% in the retrieved NO<sub>2</sub> mixing ratios.

Because we are collecting only a fraction of the fluorescence by employing the gated counting technique, factors such as changes in pressure and the timing of the delayed gate can contribute to the uncertainty. Two issues surround the timing of the delayed gate simple jitter and long-term drift. Simple jitter in the timing is a precision-related issue and will not be noticeable on top of the random noise already incurred by counting statistics. Long-term drift in the gate delay could lead to systematic errors in the measurement (if it went unnoticed). Using the fluorescence lifetime of NO<sub>2</sub>\* at 3.5 Torr of 150 ns, we calculate that a drift of 10 ns in the timing of a 750-ns-wide gate would lead to a 5% change in the integrated fluorescence collected.

We have found from preliminary experiments that the sensitivity is relatively insensitive to small changes in pressure about the operating pressure. For a pressure range of  $\pm 35\%$  centered about 3.5 Torr (the pressure at which the gated counting scheme was optimized for), the sensitivity decreased by 2%. The sensitivity becomes a stronger function of pressure for changes greater than 35%. Our pressure measurements have an absolute uncertainty of 0.1 Torr (100 Torr manometer, MKS) which translates to an uncertainty of 3% in the pressure and therefore an uncertainty of less than 1% in the NO<sub>2</sub> mixing ratios. The precision of the pressure measurements lead us to believe that the cell pressure, which is maintained by flowing through a pinhole, is constant to better than 1%. In future experiments, we plan to use a 10 Torr full-scale pressure sensor, further reducing uncertainties associated with pressure measurement to less than 0.1% in the NO<sub>2</sub> mixing ratio.

A final consideration is how changes in the molecular line width (e.g., temperature-dependent population changes and pressure broadening) or changes in the laser line width affect the excitation rate. The temperature dependence of the absolute cross section for the rovibronic feature at 17 086.5 cm<sup>-1</sup> is estimated from the partition function to be on the order of 0.5%/degree Kelvin which compares well with observations by Perkins of the temperature dependence of the fluorescence signal.<sup>46</sup> Since we measure the temperature to better than 1 K, this effect is accurately accounted for. We do not make adjustments for variations in pressure broadening or to the laser line width, since these are unimportant under the controlled conditions of a ground-based instrument.

One measure of the short-term precision is the difference between adjacent data points from observations so long as the data rate is fast compared with atmospheric variation. If the atmosphere is essentially constant over the time between two adjacent data points, then the difference between those two points is due to the instrumental noise. The size and variation of this noise becomes the limit of the instrumental precision on the same time scale. The distribution of the normalized difference between

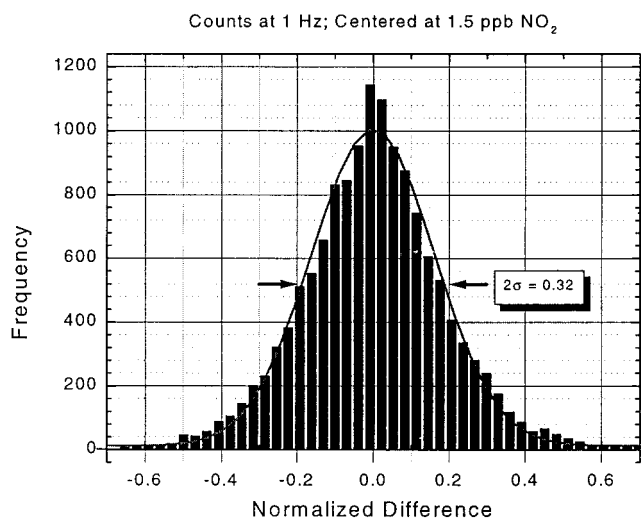


Figure 7. Distribution of normalized adjacent differences of raw counts obtained in Nashville, TN during a period when NO<sub>2</sub> concentrations varied between 0.7 and 2.3 ppb. Gaussian fit yields a standard deviation of 0.16 (half of the  $2\sigma$  width) for the data set centered at an NO<sub>2</sub> concentration of 1.5 ppb. Therefore, an upper limit to instrument precision ( $1\sigma$ ) at 1.5 ppb and at 1 Hz is 16%.

adjacent data points, i.e.,

$$\frac{[\text{NO}_2]_n - [\text{NO}_2]_{n-1}}{\sqrt{[\text{NO}_2]_n [\text{NO}_2]_{n-1}}} \quad (10)$$

should be a Gaussian if the instrumental noise is purely random, and the standard deviation of the distribution is the percent precision in a measurement ( $1\sigma$ ). Figure 7 shows the distribution of the normalized difference of adjacent raw counts collected at 1 Hz during the Nashville field campaign. The data were selected from a 4-h period on June 20, 1999 when NO<sub>2</sub> mixing ratios were between 0.7 and 2.3 ppb. The noise of the instrument is purely random as evidenced by the Gaussian fit to the adjacent difference distribution. This demonstrates that the instrument is free from any significant tailing effects or systematic noise at these mixing ratios. The standard deviation associated with the Gaussian fit is an upper limit, due to the presence of atmospheric variations, of the percent precision of the instrument at the center of this concentration range (1.5 ppb). The upper limit of the instrument precision at 1.5 ppb NO<sub>2</sub> is therefore  $\pm 16\%$  ( $1\sigma$ ) in 1 s. The precision calculated from photon counting statistics ( $(\sqrt{\text{counts}/\text{counts}}) \times 100\%$ ) for this same data set is 12%. The difference between the two different approaches is reasonably attributed to atmospheric variation on the 1-s time scale. We conclude the precision of our instrument is shot-noise-limited.

## RESULTS FROM THE FIELD

Performance of the NO<sub>2</sub>-LIF instrument under tropospheric conditions has been tested during two field deployments, one in the foothills of the Sierra Nevada (July 25–October 31, 1998) and the other in Nashville, TN as part of the Southern Oxidants Study, 1999 (SOS '99, June 15–July 15, 1999). Instrument performance is summarized for the two campaigns in Table 1.

The first deployment was from July 25 through October 31, 1998 at a research site located on a ponderosa pine plantation in

Table 1. Instrument Performance in the Field

Campaign	Dates	Calibration Constant <sup>a</sup>	Zero Uncertainty (30 s)	Detection Limit <sup>b</sup> (S/N = 2,100 mW)
Blodgett Forest	July 25 – Oct. 31, 1998	counts/ppt	ppt	ppt
Nashville, TN	June 15–July 15, 1999	0.450	18	85
		0.600	4	15

<sup>a</sup> Calibration constants are given for 100 mW of laser power, and 10-s integration period. The standard deviations of the calibration constants obtained over the duration of the campaign are given. <sup>b</sup> The detection limit is calculated for 100 mW of laser power, 10-s integration time, and a signal-to-noise of 2.

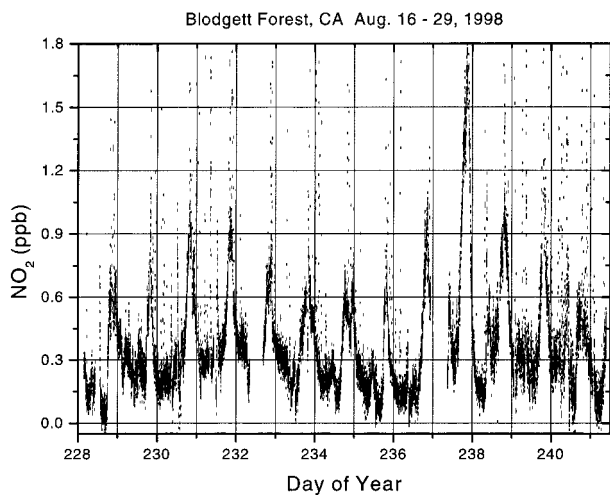


Figure 8. NO<sub>2</sub> concentration plotted as 30-second averages versus time for the two-week period, August 16–29, 1998 at UC Blodgett Forest Research Station. Points that are far from the mean are due to air from the site's diesel generator.

the Sierra Nevada foothills 50 miles east of Sacramento, CA, at a 4000-ft elevation that is owned and operated by Sierra Pacific Industries. The plantation is adjacent to Blodgett Forest in Georgetown, CA, an experimental forest managed by the College of Natural Resources and the Department of Environmental Science and Policy Management, UC, Berkeley. The site is characterized by nearly free tropospheric mixing ratios of most anthropogenic hydrocarbons, high concentrations of biogenic emissions and O<sub>3</sub>, and variable NO<sub>x</sub> and NO<sub>y</sub>. The meteorology at the site is characterized by upslope flow during the day and downslope flow at night. Other measurements at the site included NO and NO<sub>y</sub> (see papers forthcoming), O<sub>3</sub>, CO<sub>2</sub>, and H<sub>2</sub>O fluxes, a suite of biogenic and anthropogenic hydrocarbons, and pertinent meteorological parameters.<sup>56,57</sup> Figure 8 shows measured NO<sub>2</sub> in 30-second averages from a 14-day period, August 16–29, 1998. The period was characterized by the very stable meteorology described above, with NO<sub>2</sub> levels peaking in the late evening as the polluted air from the Sacramento valley reached the site followed by the clean air from the Sierra Nevada through the night. NO<sub>2</sub> levels dropped through the night, reaching their minimum near 10 am when the winds reverse and come from the Sacramento valley again.

For the Blodgett deployment, the core of the instrument was packaged in two weatherproof boxes and was operated outside

(56) Schade, G. W.; Goldstein, A. H.; Lamanna, M. S. *Geophys. Res. Lett.* **1999**, *26*, 2187–2190.

(57) Lamanna, M. S.; Goldstein, A. H. *J. Geophys. Res.* **1999**, *104* (D17), 21247–21262.

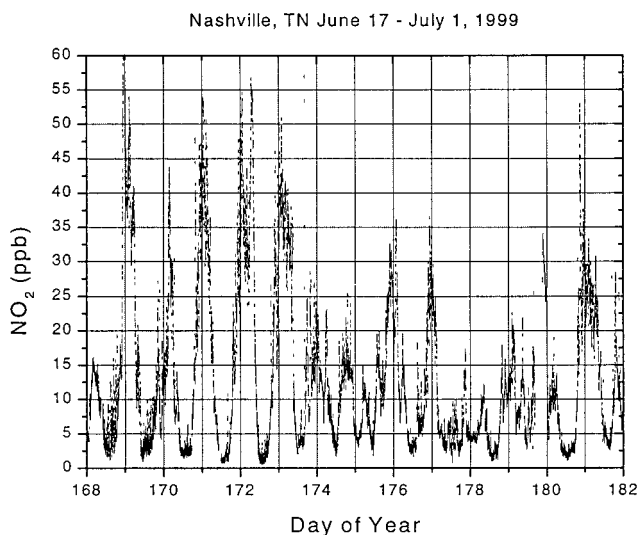


Figure 9. NO<sub>2</sub> concentration plotted as 1-minute averages versus time for the two week period, June 16–July 1, 1999 at Cornelia Fort Airpark, during the SOS '99 Nashville, TN Field Study.

at the base of a measurement tower. After an initial period devoted to improving the stability of the instrument against the large diurnal temperature swings characteristic of the site, the instrument performed well and required little maintenance. The calibration factors measured by standard addition varied slowly (less than 2% over a several hours) and were constant to within  $\pm 15\%$  for a period of 12 weeks. Routine maintenance included laser dye changes (every 2–3 weeks), data retrieval (daily), and changes in alignment of the dye laser (a few times a week). We are currently using these measurements to study the local photochemical ozone production and the regional ozone production efficiency at our site using combined measurements of O<sub>3</sub>, NO, NO<sub>2</sub> and NO<sub>y</sub>. Following this deployment, a number of improvements were made to optimize the instrument performance. These improvements decreased the laser scatter (i.e., noise) and increased the signal.

The NO<sub>2</sub>-LIF instrument was deployed from June 15 to July 15, 1999 as part of SOS '99 in Nashville, TN. The instrument contributed to the extensive suite of chemical measurements being made at the Cornelia Fort Airpark ground-based site located 8 km northeast of downtown Nashville. For information regarding the SOS '99 study please refer to <http://www.al.noaa.gov/WWWHD/pubdocs/SOS/SOS99.html>. Figure 9 shows 1-min averages of 1 Hz data collected during the month-long campaign. The instrument, in its standard equipment rack, was housed in an air-conditioned trailer located at the base of a measurement tower. The urban environment showed strong local sources, with

the majority of changes in NO<sub>2</sub> concentration being due to changes in the boundary layer height.

#### CONCLUSIONS

We have described a sensitive (15 ppt/10 s), specific, portable, and autonomous LIF instrument capable of measuring NO<sub>2</sub> throughout the troposphere. The instrument precision is governed by photon counting statistics ( $\pm 50\%$  in 10 s at 10 ppt) in the short-term, the long-term precision is better than 7% ( $2\sigma$ ), and the instrument accuracy is  $\pm 5\%$  ( $1\sigma$ ). The instrument has been operated continuously in two field campaigns, one in the foothills of the Sierra Nevada and the other near downtown Nashville, TN, during both of which no evidence was found for the existence of interferences. In the future we plan to improve the signal collection by using larger diameter optics and by more efficient collection and imaging of the illuminated volume. We will obtain a factor of 2 in optical throughput simply by using larger diameter optics. This improvement, together with higher reflectivity White-Cell mirrors, higher average laser power, and a longer delay before counting, will allow us to obtain better statistics on the uncertainty

in the zero measurement by increasing the raw signal and decreasing the laser-induced scatter contribution to the background. Finally, we plan to reduce the size and weight of the instrument to be less than 0.1 m<sup>3</sup> and weigh less than 100 kg as the necessary developments in laser, photon counting, and computer technologies become available.

#### ACKNOWLEDGMENT

This work was supported by the Office of Science, U.S. Department of Energy under Contract no. DE-AC03-76SF00098, through the UC Energy Institute, and by NASA, through its Instrument Incubator Program under Contract no. NAS1-99053. Observations in Nashville, TN were supported by the NOAA Office of Global Programs under Grant no. NA96-GP0482.

Received for review August 5, 1999. Accepted November 2, 1999.

AC9908905